A UHF 1.3 cm^2 Passive Subharmonic Tag With a 13 m Read-Range

Nicolas Casilli, *Graduate Student Member, IEEE*, Luca Colombo, *Member, IEEE*, and Cristian Cassella, *Member, IEEE*

***Abstract*— This work reports on the design and performance of the first single-antenna subharmonic tag (SA-SubHT) of its kind. Thanks to the high-quality factor of its planar electrically small antenna (ESA) and to the advantageous nonlinear dynamics enabled by the adoption of two nonlinear components in its circuit, the reported SA-SubHT exhibits an exceptionally low-power threshold ($P_{th} = -18$ dBm). Such a low P_{th}-value is achieved regardless of the extraordinarily small size of the reported SA-SubHT (its area is only 1.3 cm^2), which has been built onto a 12.4 × 10.6 × 1.6 mm^3 FR-4 printed circuit board (PCB) and uses a ultrahigh-frequency (UHF) ESA occupying just 78 mm^2. When using an effective isotropic radiated power (EIRP) at 890 MHz of +36 dBm for its interrogation in an uncontrolled electromagnetic environment, the reported two-varactor SA-SubHT generates a subharmonic response at 445 MHz detectable from more than 13 m away from its interrogating device. This read-range exceeds by more than three times the distance the same SA-SubHT on an identical PCB covers when the second varactor is replaced by an equivalent linear capacitor with a nominal capacitance identical to the varactor's zero-bias capacitance. The reported SA-SubHT creates new exciting possibilities to implement a fine-grained remote sensing through the deployment of a large number of SA-SubHTs.**

***Index Terms*— Electrically small antennas (ESAs), Internet-of-Things, nonlinear dynamics, subharmonic tags (SubHTs).**

I. Introduction

THE Internet of Things is becoming ubiquitous and many recently emerged applications would tremendously benefit from fine-grained sensing capabilities ensuring long reading distances [1], [2], [3], [4]. For instance, there is a considerable interest in developing localization strategies to improve the reliability of automated-guided vehicles [5], achieving long-range wireless sensing capabilities in harsh environments [6], [7], and performing target acquisition of objects with extremely low radar cross sections [8]. Unfortunately, the sensitivity and reading range of most commercially available passive, printable, and chip-less wireless sensing nodes (WSNs) are heavily degraded by multipath, self-interference, and clutter since their output and interrogation frequencies are the same. Additionally, attempts to miniaturize these types of WSNs for the sake of enabling a higher spatial resolution result in an unsustainable degradation of sensitivity and consequently reading range [9].

A new type of WSNs, namely the subharmonic tags (SubHTs), has recently emerged, generating new resources to produce long-range remote sensing capabilities with sensing performance immune from multipath, clutter, and readers' self-interference [10]. SubHTs rely on the nonlinear dynamics of varactor-based passive circuits to transmit sensed information at half of the interrogating frequency (f_{in}). In particular, when the received interrogation signal exceeds SubHTs' power threshold (P_{th}), an internal subharmonic oscillation is triggered in SubHTs' circuit, activating a 2:1 frequency division [11].

Differently from harmonic tags (HTs) [18], [19], which leverage polynomial nonlinearities to generate backscattered signals at twice their interrogation frequency, SubHTs can address both continuous and threshold-sensing functionalities. When assuming the same f_{in}, SubHTs' output frequency is four times lower than their HT counterparts. Therefore, HTs' output signal typically undergoes a 12 dB higher path-loss compared to SubHTs' output signal. This 12 dB difference contributes to HTs' reading ranges being typically lower than those achievable by SubHTs [10]. Even more, SubHTs can implement a memory functionality without requiring ad hoc memory components [3], [10]. Up to date, all the prior demonstrated SubHTs rely on two-port networks, featuring a set of lumped components and two separate antennas to satisfy the resonance conditions for the activation of the subharmonic oscillation in their circuit [11]. This approach increases the size of SubHTs, adversely impacting scalability, integration, and, consequently, their implementation as remote sensing devices.

In this letter, we present the first high sensitivity single-antenna SubHT (SA-SubHT), which operates in the ultrahigh-frequency (UHF) range and has an extremely compact form factor (it occupies only a 1.3 cm^2 area, Fig. 1). The topology of this SA-SubHT embodies a single electrically small antenna (ESA) coupled with a parametric frequency divider (PFD) that exploits the nonlinear dynamics of two varactor diodes to activate the generation of the subharmonic response. To the best of our knowledge, the SA-SubHT presented in this work grants the longest reading range ever achieved by passive tags relying on ESAs (see Table I). In Section II, we will first discuss the principle of operation of SA-SubHTs. Then, the experimental methods used to characterize the SA-SubHT will be discussed, along with a

Manuscript received 27 February 2023; revised 15 April 2023; accepted 15 April 2023. This work was supported by the National Science Foundation Comms Circuits and Sens Sys (CCSS) Program under Award 1854573. *(Corresponding author: Nicolas Casilli.)*

The authors are with the SMART Center, Department of Electrical and Computer Engineering, Northeastern University, Boston, MA 02115 USA (e-mail: casilli.n@northeastern.edu; l.colombo@northeastern.edu; c.cassella@northeastern.edu).

This article was presented at the IEEE MTT-S International Microwave Symposium (IMS 2023), San Diego, CA, USA, June 11–16, 2023.

Color versions of one or more figures in this letter are available at https://doi.org/10.1109/LMWT.2023.3268542.

Digital Object Identifier 10.1109/LMWT.2023.3268542

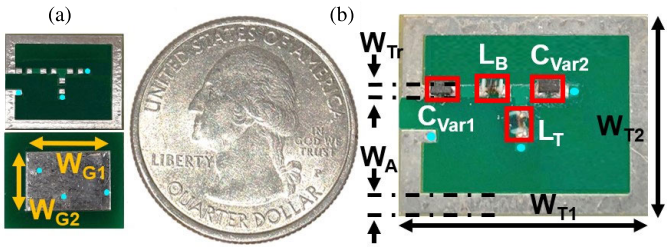

Fig. 1. (a) Image of the front and back views of the bare PCB of the SA-SubHT adjacent to a U.S. quarter dollar coin used as a reference for its size. (b) Image of the built SA-SubHT showing soldered lumped components and feature sizes of the traces, ESA, and total board (W_A = 48 mil, W_{T_1} = 496 mil, W_{T_2} = 408 mil, W_{T_r} = 24 mil, W_{G_1} = 340 mil, and W_{G_2} = 240 mil). The aqua-blue markings indicate the locations of through-hole vias connecting the top metal layer to the partial ground plane.

TABLE I

COMPARISON TABLE SHOWING THE PERFORMANCE OF VARIOUS PASSIVE SENSING TAGS SPANNING SEVERAL FREQUENCY RANGES

Device	f_{in}	λ	d_{max}	Area	EIRP
This Work	*890 MHz*	*0.34 m*	*13.5 m*	$0.001\lambda^2$	*+36 dBm*
[3] (SubHT)	*870 MHz*	*0.35 m*	*4 m*	$0.078\lambda^2$	*+26 dBm*
[10] (SubHT)	*886 MHz*	*0.38 m*	*4.5 m*	$0.066\lambda^2$	*+37 dBm*
[12] (SubHT)	*790 MHz*	*0.34 m*	*4 m*	$0.082\lambda^2$	*+36 dBm*
[13]	*915 MHz*	*0.33 m*	*0.4 m*	$0.012\lambda^2$	*+30 dBm*
[14]	*1.59 GHz*	*0.19 m*	*1.5 m*	$1.197\lambda^2$	*+10 dBm*
[15]	*6.5 GHz*	*0.05 m*	*1.4 m*	$0.080\lambda^2$	*+30 dBm*
[16]	*2.5 GHz*	*0.12 m*	*0.5 m*	$0.056\lambda^2$	*+12 dBm*
[17]	*1.04 GHz*	*0.29 m*	*1.0 m*	$0.004\lambda^2$	*+15 dBm*

comparison of the performance of the presented SA-SubHT with a SA-SubHT featuring only a single varactor.

II. DESIGN AND ANALYSIS

The SA-SubHT tag presented in this work is designed to operate with an interrogation frequency (f_{in}) of 890 MHz and an output frequency (f_{out}) of 445 MHz. A schematic of the proposed system is reported in Fig. 2. This SubHT consists of an ESA, with an inductive input impedance (Z_A), coupled to a one-port PFD with a frequency-dependent input impedance (Z_P). The PFD is composed by a series varactor (C_{Var1}), a series inductor (L_B), and the parallel between a second varactor (C_{Var2}) and a second inductor (L_T).

In two-port SubHTs topologies, the satisfaction of four resonance-conditions permits to minimize P_{th}. SA-SubHTs rely instead on the satisfaction of only three conditions. In particular, to generate the lowest possible P_{th}, it is critical to make the series of Z_A and Z_P resonate at both f_{in} and f_{out}. The third condition involves maximizing the voltage swing across the nonlinear elements to generate a large parametric modulation of the impedance in the circuit. In this regard, having two nonlinear capacitors permits to increase the effective impedance modulation in the circuit for any received power level, greatly reducing the P_{th} value required to activate the frequency division. To satisfy the three resonance conditions for the SA-SubHT reported in this work, L_T and C_{Var2} were chosen to produce, together with C_{Var1} and L_B, a series

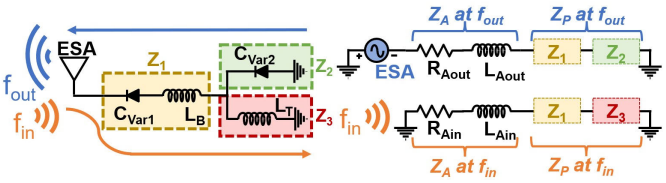

Fig. 2. Schematic representation of the SA-SubHT reported in this work. The interrogation signal is received by an ESA and a frequency divided output signal is transmitted by the same ESA. A set of lumped components ensures the satisfaction of the resonance-conditions leading to a P_{th}-minimization using just two meshes. The model numbers for the lumped components are: C_{Var1}: SMV1430-040LF (1.24 pF with tuning range = 30%), L_B: 0402DC-4N6XGR (4.6 nH), C_{Var2}: SMV1405-040LF (2.7 pF with tuning range = 40%), and L_T: 0402DC-22NXGR (22 nH).

resonance at both f_{in} and f_{out} (Fig. 2). Hyperabrupt varactors were used to maximize the achievable capacitive tuning range.

The employed ESA consists of a planar square loop antenna built on an FR-4 substrate with a circumference of $0.12 \cdot \lambda_{\text{in}}$, where λ_{in} is the electromagnetic wavelength of the interrogation frequency in the substrate. This antenna structure inherently exhibits an inductive input impedance with a relatively low dependence of its equivalent inductance against frequency [20]. The selection of a loop antenna reduces the SA-SubHT's overhead area as the components required to synthesize Z_P can be placed within the loop's perimeter without substantially perturbing the radiation characteristics of the antenna. Front- and back-view pictures of the built SA-SubHT, including the ESA and the layout of the soldered components are reported in Fig. 1. The designed ESA's input impedance values at f_{in} and f_{out} were simulated through finite-element (FE) methods as $(1 + j \cdot 160)\ \Omega$ (R_{Ain} and $j\omega L_{Ain}$) and $(0.1 + j \cdot 60)\ \Omega$ (R_{Aout} and $j\omega L_{Aout}$).

Such a low resistance forming Z_A is a clear indication of our ESA's suboptimal radiation efficiency, as expected based on its small form-factor. All things considered, using low radiation resistance antennas (e.g., antennas with a high radiation quality factor) in SubHTs reduces the losses that the parametric gain generated from the capacitance modulation of the adopted varactors must compensate to trigger the subharmonic oscillation [11], [20]. For this reason, using an ESA in SA-SubHTs enables a partial compensation of SA-SubHTs' reduced antenna gain due to miniaturization. The gain of the antenna used by the reported SA-SubHT was found to be -12.5 dBi at f_{in} and -15.4 dBi at f_{out} through FE analysis. As anticipated for a miniaturized loop antenna, the radiation characteristics conform to a two-lobe structure with its maxima located in the plane of the printed loop [20]. The same FE methods have also confirmed that only the SA-SubHT's portion not covered by the bottom grounded plate contributed to radiation. This feature allows to quantify the area of the radiating portion of our SA-SubHT as 78 mm^2. The antenna circuit parameters and radiation pattern of the ESA can be found in Fig. 3. The estimations of the input impedances and intrinsic gain levels permitted us to utilize the power auxiliary generator (pAG) technique to predict P_{th} and calculate the maximum distance of detection (d_{max}) for the simulated and designed SA-SubHT. Using this *pAG* method

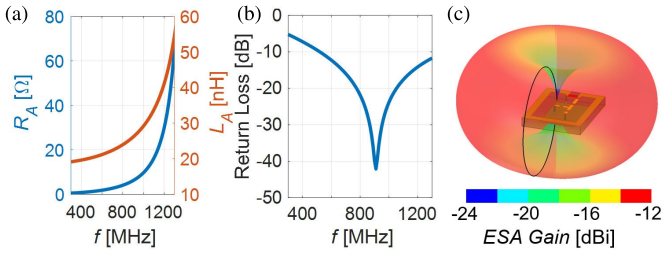

Fig. 3. (a) Simulated input impedance for the ESA. As seen, the small antenna resistance indicates poor radiation performance. However, the relatively large inductive impedance contributes to increasing the overall quality factor of the SA-SubHT, consequently reducing P_{th}. Using FE methods, the designed ESA's input impedance values at f_{in} and f_{out} were determined as $(1+j\cdot 160)\ \Omega$ ($R_{A\text{in}}$ and $j\omega L_{A\text{in}}$) and $(0.1+j\cdot 60)\ \Omega$ ($R_{A\text{out}}$ and $j\omega L_{A\text{out}}$). (b) Simulated return loss of the ESA when Z_P equals the conjugate of Z_A at the interrogation frequency. (c) Simulated radiation pattern at 890 MHz.

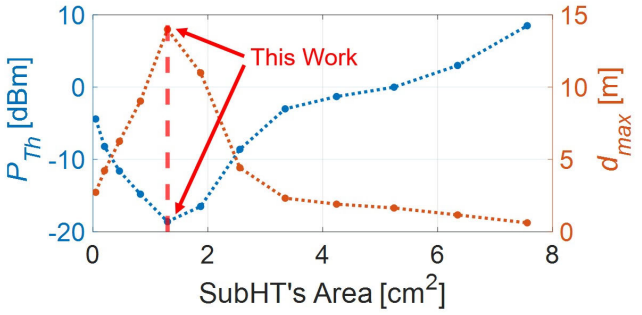

Fig. 4. FEM-simulated optimal P_{th} and d_{max} trends (in blue and orange, respectively) versus the SubHT's area using the pAG technique.

also enabled design compensation for any degradations of P_{th} due to layout parasitics and undesired deviations in component values compared to the nominal ones [21]. We also used this technique to simulate the optimal performance of our SubHT (see Fig. 4) when scaling its area (hence the area of its ESA) while maintaining the same circuit topology and quality factor for all the adopted lumped components. Evidently, making the SubHT's area smaller or larger than what was used generates significant degradations of d_{max} and P_{th}. In other words, the reported SubHT has an ideal size when targeting a large d_{max} value and the smallest possible SubHT's area.

III. Results

After designing the described SubHT, we built it onto a 12.4 × 10.6 × 1.6 mm^3 FR-4 printed circuit board (PCB) by soldering off-the-shelf lumped components (see Fig. 1). To characterize the performance of our SubHTs, we assembled a wireless setup operating in a shared laboratory. Such a setup permitted to emulate an IoT reader capable of transmitting an effective isotropic radiated power (EIRP) of +36 dBm at the interrogation frequency while showing an RF sensitivity of −115 dBm at the output frequency. Our setup consists of: 1) a signal generator (model-number: Tektronix TSG 4104A) transmitting −4 dBm and connected to a commercial ultra-wideband antenna (Aaronia HyperLOG 4025, with a gain of +4 dBi) through a power amplifier (model-number: ZHL-1000-3W+) and 2) a spectrum analyzer (model-number: Agilent ESA-E4402B) with input port connected to

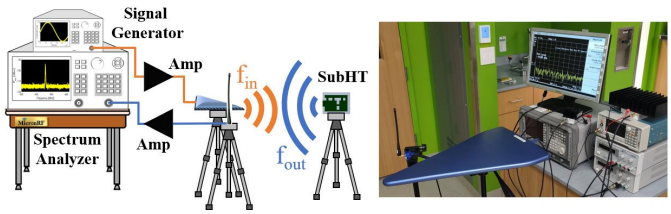

Fig. 5. Schematic view and actual image of the wireless setup used during our SubHT's characterization. This includes a signal generator delivering the interrogation signal at f_{in}, a power amplifier, the transmitting antenna, the receiving antenna, a second power amplifier, and a spectrum analyzer used as receiver. The intention for this setup was to emulate the configuration of a conventional IoT-reader. Thus, antennas and measurement tools were practically placed on top of each other.

a power amplifier (model-number: ZHL-72A+) used to boost the sensitivity of the receiver from −95 to −115 dBm. This amplifier is connected to a 450 MHz half-wavelength dipole antenna (model-number: 712-ANT-433-CW-QW, with a gain of +3.3 dBi) placed in close vicinity to the other antenna [22]. A schematic overview of the adopted setup, as well as a photo of the experimental setup, is provided in Fig. 5. To assess P_{th}, the SA-SubHT was placed onto a plastic tripod aligned with the direction of maximum gain of the transmitting antenna connected to the signal generator. The tripod was then progressively moved away from our wireless setup until a measurable response at f_{out} was no longer detected by the spectrum analyzer. The distance immediately prior to this lack of detection was recorded as our d_{max}-value. To extract P_{th}, we estimated our SA-SubHT's received power at f_{in} using the Friis free-space propagation model [23], for a distance from the signal generator equal to d_{max}.

The same analysis was repeated for several frequencies in the neighborhood of the targeted operational frequency of our SA-SubHT. As expected, our SA-SubHT shows the longest d_{max} and the lowest P_{th} at the designed frequency of 890 MHz. The d_{max} of the constructed device was 13.5 m, corresponding to a P_{th} value of −18 dBm. Table I compares the reading range and total area of the measured SA-SubHT to current state-of-the-art passive, chipless and batteryless counterparts.

To validate our design decision to adopt two nonlinear components to most efficiently modulate the reactance in the circuit, we also built another SA-SubHT on an identical PCB wherein C_{Var2} is replaced with a capacitor (C_T) exhibiting the same capacitance as the removed unbiased varactor for small signals. Then, we repeated the wireless characterization procedure we followed to characterize the performance of the SA-SubHT using two varactors to assess the P_{th} and d_{max} values of the same SA-SubHT when using only one varactor. We found that in addition to shifting the optimal interrogation frequency upward by almost 30 MHz, the P_{th} of the device was degraded by more than 10 dB, leading to reading ranges reduced by more than three times (see Fig. 6). This result shows that the inclusion of a second nonlinear component in the parametric circuit is critical for ensuring a minimized P_{th} and maximized d_{max}. When accounting for the miniaturized size of our reported SA-SubHT, the d_{max} value demonstrated in this work opens exciting scenarios toward

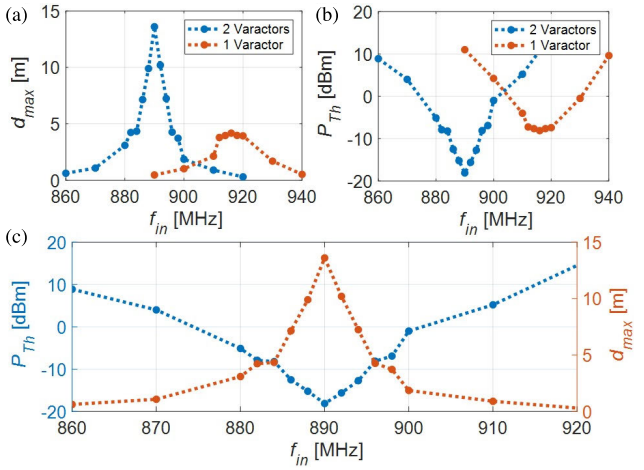

Fig. 6. Measured results for (a) $d_{\max}$ and (b) P_{th} of the proposed SA-SubHT compared to the case with a single varactor. As can be seen, the use of a single varactor instead of two degrades the performance of the system by more than 10 dB. (c) Measured $d_{\max}$ and P_{th} values for the reported double-varactor SA-SubHT. It is important to note that both the two-varactor and one-varactor SubHTs are constructed on identical PCBs using the same embedding network. The difference between the two designs is the adoption of an equivalent nonlinear capacitive element in the two-varactor SubHT in the place of the linear capacitor used in the one-varactor design.

the development of passive tags for a variety of applications, including target acquisition, tracking, remote sensing, navigation, and localization [18].

IV. Conclusion

In this letter, we presented the performance and electrical characteristics of the first ever reported SA-SubHT. Owing to its nonlinear dynamics and despite its exceptionally small size, the SA-SubHT reported in this work can achieve a P_{th} of -18 dBm, enabling reading ranges exceeding 13 m. The single-antenna design and subsequently high potential for miniaturization of this device open exciting paths toward the development of distributed wireless sensor networks for Internet of Things applications that demand a fine-grained monitoring of targeted parameters of interest.

References

[1] S. Kumar, P. Tiwari, and M. Zymbler, "Internet of Things is a revolutionary approach for future technology enhancement: A review," *J. Big Data*, vol. 6, p. 111, Dec. 2019.

[2] S. D. Glaser, "Some real-world applications of wireless sensor nodes," *Smart Struct. Mater.*, 2004, doi: 10.1117/12.539089.

[3] H. M. E. Hussein, M. Rinaldi, M. Onabajo, and C. Cassella, "Capturing and recording cold chain temperature violations through parametric alarm-sensor tags," *Appl. Phys. Lett.*, vol. 119, no. 1, Jul. 2021, Art. no. 014101.

[4] J. Zhan, G. Y. Tian, A. M. J. Marindra, A. I. Sunny, and A. B. Zhao, "A review of passive RFID tag antenna-based sensors and systems for structural health monitoring applications," *Sensors*, vol. 17, no. 2, p. 265, 2017.

[5] R. Chakma et al., "Navigation and tracking of AGV in ware house via wireless sensor network," in *Proc. IEEE 3rd Int. Electr. Energy Conf. (CIEEC)*, Beijing, China, Sep. 2019, pp. 1686–1690.

[6] S. Duobiene et al., "Development of wireless sensor network for environment monitoring and its implementation using SSAIL technology," *Sensors*, vol. 22, no. 14, p. 5343, Jul. 2022.

[7] A. I. Sunny, A. Zhao, L. Li, and S. K. K. Sakiliba, "Low-cost IoT-based sensor system: A case study on harsh environmental monitoring," *Sensors*, vol. 21, no. 1, p. 214, Dec. 2020.

[8] R. Maggiora, M. Saccani, D. Milanesio, and M. Porporato, "An innovative harmonic radar to track flying insects: The case of *Vespa velutina*," *Sci. Rep.*, vol. 9, no. 1, p. 11964, Aug. 2019.

[9] A. K. Skrivervik, J.-F. Zürcher, O. Staub, and J. R. Mosig, "PCS antenna design: The challenge of miniaturization," *IEEE Antennas Propag. Mag.*, vol. 43, no. 4, pp. 12–27, Aug. 2001.

[10] H. M. E. Hussein, M. Rinaldi, M. Onabajo, and C. Cassella, "A chip-less and battery-less subharmonic tag for wireless sensing with parametrically enhanced sensitivity and dynamic range," *Sci. Rep.*, vol. 11, no. 1, p. 3782, Feb. 2021.

[11] H. M. E. Hussein, M. A. A. Ibrahim, G. Michetti, M. Rinaldi, M. Onabajo, and C. Cassella, "Systematic synthesis and design of ultralow threshold 2:1 parametric frequency dividers," *IEEE Trans. Microw. Theory Techn.*, vol. 68, no. 8, pp. 3497–3509, Aug. 2020.

[12] H. M. E. Hussein, L. Colombo, and C. Cassella, "A $LiNbO_3$-based subharmonic tag for passive and far-field identification," in *Proc. IEEE 35th Int. Conf. Micro Electro Mech. Syst. Conf. (MEMS)*, Tokyo, Japan, Jan. 2022, pp. 1022–1025.

[13] C. L. Baumbauer et al., "Printed, flexible, compact UHF-RFID sensor tags enabled by hybrid electronics," *Sci. Rep.*, vol. 10, no. 1, p. 16543, Oct. 2020.

[14] B. Kubina, J. Romeu, C. Mandel, M. Schüßler, and R. Jakoby, "Quasi-chipless wireless temperature sensor based on harmonic radar," *Electron. Lett.*, vol. 50, no. 2, pp. 86–88, Jan. 2014.

[15] S. Deshmukh and H. Huang, "Wireless interrogation of passive antenna sensors," *Meas. Sci. Technol.*, vol. 21, no. 3, 2010, Art. no. 035201.

[16] A. Vena, E. Perret, and S. Tedjini, "Chipless RFID tag using hybrid coding technique," *IEEE Trans. Microw. Theory Techn.*, vol. 59, no. 12, pp. 3356–3364, Dec. 2011.

[17] V. Palazzi et al., "Demonstration of a chipless harmonic tag working as crack sensor for electronic sealing applications," *Wireless Power Transf.*, vol. 2, no. 2, pp. 78–85, Sep. 2015.

[18] M. Saikat, K. Deepak, and C. Premjeet, "Recent advances and applications of passive harmonic RFID systems: A review," *Micromachines*, vol. 12, p. 420, Apr. 2021.

[19] R. Raju and G. E. Bridges, "A compact wireless passive harmonic sensor for ammonia sensing in packaged food," *IEEE Sensors Lett.*, vol. 6, no. 4, pp. 1–4, Apr. 2022.

[20] C. A. Balanis, *Antenna Theory: Analysis and Design* (The Harper and Row Series in Electrical Engineering). New York, NY, USA: Wiley, 1982.

[21] C. Cassella and G. Piazza, "Low phase-noise autonomous parametric oscillator based on a 226.7 MHz AlN contour-mode resonator," *IEEE Trans. Ultrason., Ferroelectr., Freq. Contr.*, vol. 62, no. 4, pp. 617–624, Apr. 2015.

[22] S. S. Park, "An IoT application service using mobile RFID technology," in *Proc. Int. Conf. Electron., Inf., Commun. (ICEIC)*, Honolulu, HI, USA, Jan. 2018, pp. 1–4.

[23] H. T. Friis, "A note on a simple transmission formula," *Proc. IRE*, vol. 34, no. 5, pp. 254–256, May 1946.